Estuarine, Coastal and Shelf Science 217 (2019) 28–36

Contents lists available at ScienceDirect

Estuarine, Coastal and Shelf Science

journal homepage: www.elsevier.com/locate/ecss

Saltwater intrusion in a subtropical estuary

Gisselle E. Guerra-Chanis[a,c,*], Miguel Á. Reyes-Merlo[b], Manuel Díez-Minguito[b], Arnoldo Valle-Levinson[a]

[a] Department of Civil and Coastal Engineering, University of Florida, Gainesville, FL, 32611, USA
[b] Instituto Interuniversitario de Investigación Del Sistema Tierra en Andalucía (IISTA), Universidad de Granada, Avda. Del Mediterráneo, S/n, E-18006, Granada, Spain
[c] Centro de Investigaciones Hidráulicas e Hidrotécnicas, Universidad Tecnológica de Panamá, Panamá

ARTICLE INFO

Keywords:
Saltwater intrusion
Climate change
Markov-chain model
Suwannee River

ABSTRACT

River discharge, precipitation, wind, water level and salinity measurements were used to investigate saltwater intrusion in a subtropical estuary. The upstream limit of saltwater intrusion was defined by the position of the 2 g/kg isohaline (X_2) as it changed each tidal cycle. Observations were obtained from November 2014 to November 2015 along the Suwannee River, at Florida's Big Bend. Observations provided information to construct a first-order autoregressive Markov-chain model and predict X_2. The model predicts X_2 from its position in the previous tidal cycle, from river discharge, from water level, from precipitation and from wind velocity. In order to capture the seasonality of the Suwannee River discharge, the analysis was done separately for high and low river discharge regimes. The high discharge regime for the particular year of observations coincided with the cold season and had a mean value of 360 m^3/s. The low discharge regime overlapped with the warm season and had a mean of 198 m^3/s. As expected, saltwater intrusion was inversely related to river discharge. Values of X_2 were 0.4 km for a discharge of 377 m^3/s, and 6 km for a discharge of 195 m^3/s. The autoregressive model was able to reproduce the observed seasonality of saltwater intrusion in the Suwannee River. The model was then used to project values of X_2 for different scenarios of climate change as represented by possible combinations of river discharge and water levels.

1. Introduction

Saltwater intrusion limits the availability of freshwater for human consumption (Crain et al., 2004; Neubauer, 2013), affects the distribution of estuarine vegetation (Neubauer, 2013), and can impact human health (Vineis et al., 2011). The limit of intrusion responds to various forcing factors. River discharge continuously adds freshwater, while gravitational circulation and oscillatory tidal dispersion drives ocean water into the estuary (Fischer, 1976). Remote forcing, in the form of increased water levels, can also transport salt into an estuary (e.g. Wong and Valle-Levinson, 2002). Such mechanisms of saltwater influx determine the length of saltwater intrusion, the residence time of sediments and pollutants, and the response time to climate forcing, e.g., changes to river discharge, tides, and winds (Monismith et al., 2002; Bowen and Geyer, 2003; Hetland and Geyer, 2004; MacCready, 2007).

Saltwater intrusion largely depends on the time scale of forcings and the response time of the estuary (Warner et al., 2005). The length of saltwater intrusion is the distance from the estuary's mouth up to the location of an isohaline of known value, customarily 2 g/kg (Jassby et al., 1995). The position of the isohaline of 2 g/kg (X_2) and river discharge Q can typically explain the saltwater intrusion through power-law relationships (Hansen and Rattray, 1965). Power-law relationships of the form $X_2 \propto Q^n$, where n is any real value, assume a quasi-steady state where the length of saltwater intrusion results from the advection of river discharge and gravitational circulation (Pritchard, 1954; MacCready, 1999; Monismith et al., 2002). Partially stratified estuaries, like the Hudson River estuary and Delaware Bay, report values of n varying from -1 to $-1/3$ for high to low river discharge, respectively (Abood, 1974; Chatwin, 1976; Monismith et al., 2002; Gong and Shen, 2011).

Numerical models (1D and 3D) can simulate the time dependence of saltwater intrusion better than power-law approximations (Chatwin, 1976; Kranenburg, 1986). A quasi-steady state occurs when the response time of the estuary is shorter than the timescale of the forcing (MacCready, 2007; Lerczak et al., 2009). Unsteadiness is related to a comparable response time of the estuary to the timescale of the forcing (Simpson et al., 2001; Lerczak et al., 2006). Results have shown that saltwater intrusion is farther upstream during spring tides than neap

* Corresponding author. Department of Civil and Coastal Engineering, University of Florida, Gainesville, FL, 32611, USA.
E-mail address: gisselle.guerra@ufl.edu (G.E. Guerra-Chanis).

https://doi.org/10.1016/j.ecss.2018.10.016
Received 26 April 2018; Received in revised form 16 October 2018; Accepted 22 October 2018
Available online 23 October 2018
0272-7714/ © 2018 Elsevier Ltd. All rights reserved.

tides for well-mixed and strongly stratified estuaries, and of shorter distance during spring tides than in neap tides for partially mixed estuaries (Gong and Shen, 2011).

The objectives of this study are a) to determine the saltwater intrusion, or the value of the 2 g/kg isohaline position (X_2), along a subtropical estuary from its salinity distribution; b) to build an autoregressive model that relates X_2 to forcing variables; and c) to use the autoregressive model to predict X_2 under different climate change scenarios represented by possible combinations of river discharge and water level rise. To address the objectives, the salinity distribution of the Suwannee River estuary, a subtropical estuary in west Florida, is used to derive X_2 and fit it to a first-order Markov-chain model. Observed values of X_2 are related to tidally averaged river discharge, water level, precipitation, wind, and X_2 of the previous tidal cycle. Following the methodology of Reyes-Merlo et al. (2013), X_2 is calculated for high and low river discharge, using a threshold river discharge from the period of analysis. Results describe the response of X_2 to different inputs of river discharge, water levels at the mouth of the river, precipitation and wind velocity.

2. Study site

The Suwannee River is the second largest river system in Florida in terms of its mean annual flow of 298 m^3/s and its drainage area of 25,770 m^2. It is 392 km long and features an average stream gradient of 7.5 cm per kilometer (Valle-Levinson, 2012; Light et al., 2002). The drainage basin encompasses the Northern Highlands and the Gulf Coastal Lowlands physiographic regions. The Highlands are generally around 30–60 m above Mean Sea Level (MSL) and include streams, lakes, and ponds. The Gulf Coastal Lowlands are 30 m above MSL and are characterized by low relief, karstic topography and a high connectivity between surface water and groundwater systems (SRWMD, 2005). The drainage of the Suwannee River ends at the Suwannee River estuary, which extends up to 16 km upstream from the mouth (Fig. 1). The estuary has a mean water depth of 2.2 m below Mean Sea Level, and is dominated by semidiurnal tides of 0.7 m range (Tuckey and Dehaven, 2006). Observations collected during low river discharge indicate that tides can reach up to 43 km upstream from the mouth (McPherson and Hammett, 1991). No study has yet documented saltwater intrusion length nor its seasonality.

The climate of the region is a mixture of warm temperate and subtropical conditions, with long (7–8 months) warm summers and short (2-3 months-long) mild winters (Crandall et al., 1999). Mean annual water temperature in the Florida portion of the watershed is 20 °C, with a range from 12 °C to 27 °C during the year. Precipitation has a bimodal distribution with peaks in March and September. The precipitation ranges from 1170 to 1520 mm, with the lowest in the upper basin (higher latitudes) and the highest closer to the Gulf coast—at lower latitudes (SRWMD, 2005). In addition to the temporal and spatial variability of rainfall across the basin, the river is also affected by the El Niño Southern Oscillation (ENSO). For example, evidence shows that river flood pulses of 1973, 1984 and 1998 in the Suwannee River were related to “moderate to strong” El Niño events (Tootle and Piechota, 2004).

Annual discharge from the Suwannee River into the Gulf of Mexico varies between the warm (May–October) and cold (November–April) seasons. Data collected at the Wilcox United States Geological Survey (USGS) station, over the period of 1942–2003, gives a mean discharge of 320 m^3/s for the warm season, 255 m^3/s for the cold season, and an overall annual mean of 288 m^3/s. During low flow conditions, groundwater from the Upper Floridian aquifer flows into the river and sustains the base flow. During high-flow conditions of heavy rainfall, river water flows into the aquifers through small cavities and conduits (Crandall et al., 1999; Katz et al., 1997).

This study addresses the salinity distribution along the Suwannee River, which until now has only been described qualitatively. Some reports (e.g., Tillis (1999); Light et al. (2002)) indicate that the salinity distribution varies temporally and spatially due to tides, river discharge, and winds. Increased upstream salinities develop during different conditions: low river discharge, high tides and during storm surges if the river discharge is low. Regularly, salinity decreases upstream and during low tides; and vertically from bottom to surface (Light et al., 2002). Vertical differences in salinity from top to bottom can reach values of up to 20 g/kg in 4 m (personal observations). This study contributes to the understanding of the salinity distribution over subtidal scales along the Suwannee River estuary.

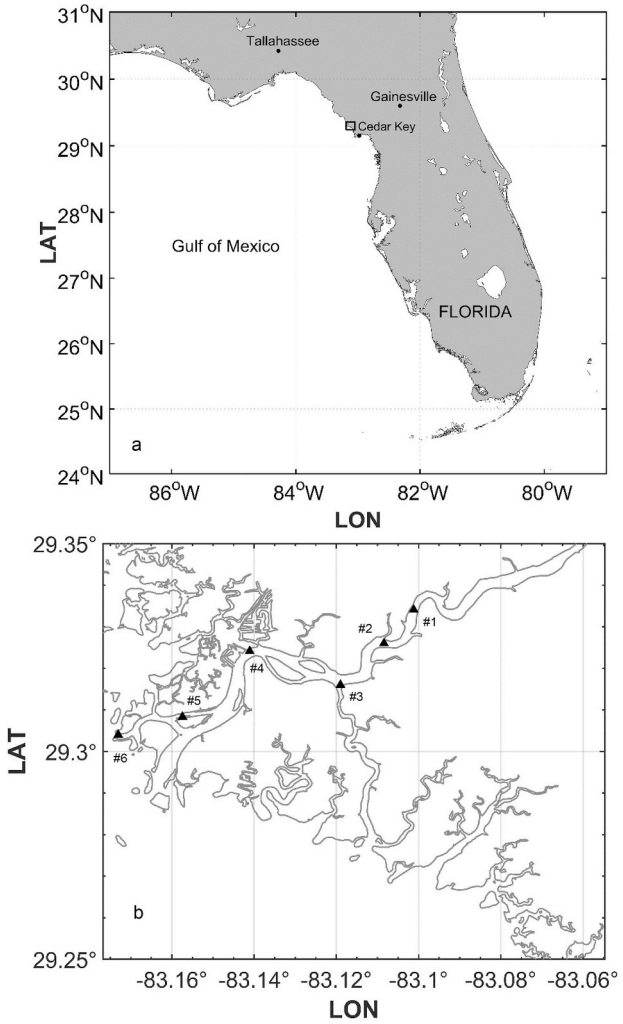

Fig. 1. Regional location of the a) Suwannee River estuary (black rectangle) and b) location of the CTD stations (filled black triangles).

3. Methods

Observations of salinity and water level were made along the Suwannee River for approximately one year from November 2014 to November 2015. Salinity measurements were used to calculate the longitudinal salinity distribution and the upstream position of the 2 g/kg isohaline (X_2). Saltwater intrusion was represented by the position of X_2 and predicted with an autoregressive model. The model predicted X_2 (dependent variable) as a function of the variability of forcings (independent variables): river discharge, water level, precipitation and wind velocity components.

Table 1
CTD stations along the Suwannee River.

Station #	latitude	longitude	Mean water depth (m)	Distance (km)
1	29° 20.165′ N	83° 6.071′ W	1.78	9.8
2	29° 19.474′ N	83° 6.505′ W	3.13	7.1
3	29° 18.901′ N	83° 7.124′ W	0.48	6.0
4	29° 19.456′ N	83° 8.464′ W	4.42	4.1
5	29° 18.484′ N	83° 9.445′ W	1.20	1.9
6 (mouth)	29° 18.241′ N	83° 10.382′ W	0.77	0

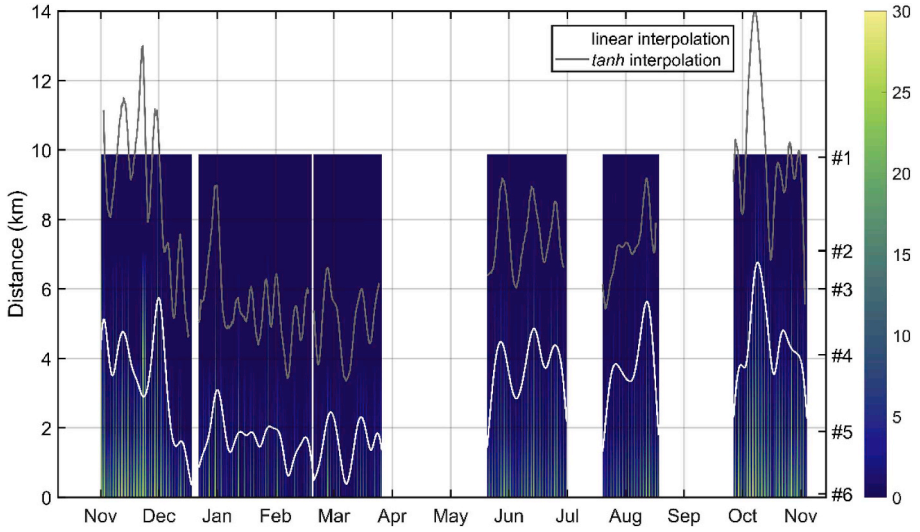

Fig. 2. Longitudinal salinity distribution at the Suwannee River from November 2014–November 2015. Contour colors indicate observed temporal (x-axis) and longitudinal (y-axis) distribution of salinity. The position of X_2 from the linear interpolation is in white color, and in gray color from the *tanh* interpolation. Locations of the CTD stations are on the right y-axis, the river's mouth is at 0 km. (For interpretation of the references to color in this figure legend, the reader is referred to the Web version of this article.)

3.1. Data collection

A measurement campaign collected salinity measurements and water levels with different types of instruments: Schlumberger Diver recorders (CTD divers) and Sea-Bird SBE26 and SBE37 recorders (CTD). The instruments were deployed from Nov 23, 2014 to Nov 22, 2015, recording time series with 3-min sampling intervals (Table 1). The CTDs were deployed on the river bed in the channel, spaced ~1.5–2.5 km (Fig. 1). Instruments were recovered and redeployed at near-monthly intervals to upload data and to clean sensors. Ancillary data consisted of time series of river discharge, precipitation and wind (Fig. 3). River discharge and precipitation time series were only available from the Wilcox Station 023323500 (29° 35′ 22″ N, 82° 56′ 12″ W), located ~43 km upstream from the Suwannee River's mouth. River discharge values had a sampling interval of 15 min, available from US Geologic Survey (USGS) site https://waterdata.usgs.gov/nwis. Precipitation data consisted of daily measurements collected by the Suwannee River Water Management District (SRWMD). Raw data are available at http://www.mysuwanneeriver.org/realtime/rain-levels.php. In addition, 10-min wind speeds and directions were obtained from the meteorological station #CDRF1 at Cedar Key, FL ~23 km to the southwest of the river's mouth. Wind data are available at http://www.ndbc.noaa.gov/station_history.php?station=cdrf1.

3.2. Data analysis

Intratidal variations were removed from the river discharge record by using a low-pass Lanczos filter centered at 30 h. Wind vectors were decomposed into north and east components. These wind components were smoothed with a low-pass Lanczos filter centered at 70 h to remove periods shorter than 2 days, including inertial oscillations. The water elevation was demeaned before applying a complex demodulation (Thomson and Emery, 2014) to extract the amplitude of the semidiurnal tide. This represented a de-tided water level, which is henceforth referred to as “water level”. Raw data for precipitation were linearly interpolated to coincide with the time of river discharge, wind velocities, and water level.

Absolute Salinity was estimated using conductivity, temperature and pressure data from the CTDs using the Thermodynamic Equation of Seawater – TEOS 2010 (T. J. McDougall and Barker, 2011; T. C. McDougall et al., 2012). Longitudinal salinity distributions were calculated from the six stations along the Suwannee River estuary (Fig. 1b) by two approaches, a linear interpolation and a hyperbolic tangent interpolation (*tanh* interpolation). Before doing the interpolations, recorded salinities were first tidally averaged from bottom measurements (e.g., Monismith et al., 2002).

The position of the tidally averaged isohaline of 2 g/kg represents the length of saltwater intrusion, referred throughout this study as X_2. For the linear interpolation approach, an X_2 representative for each tidal cycle was determined from a semidiurnal complex demodulation. The alternate approach follows previous studies that have assumed a longitudinal distribution of salinity following a hyperbolic tangent shape (Chatwin, 1976; Hansen and Rattray, 1965). Such distribution assumption is effective when there is no spatial resolution for the salinity distribution due to insufficient measurement stations (Warner et al., 2005). In this study, we tested this approach by implementing the hyperbolic tangent interpolation using salinity measurements and calculating the position of X_2.

Following Warner et al. (2005), the *tanh* interpolation followed a sigmoid salinity distribution along the estuary $S(x)$:

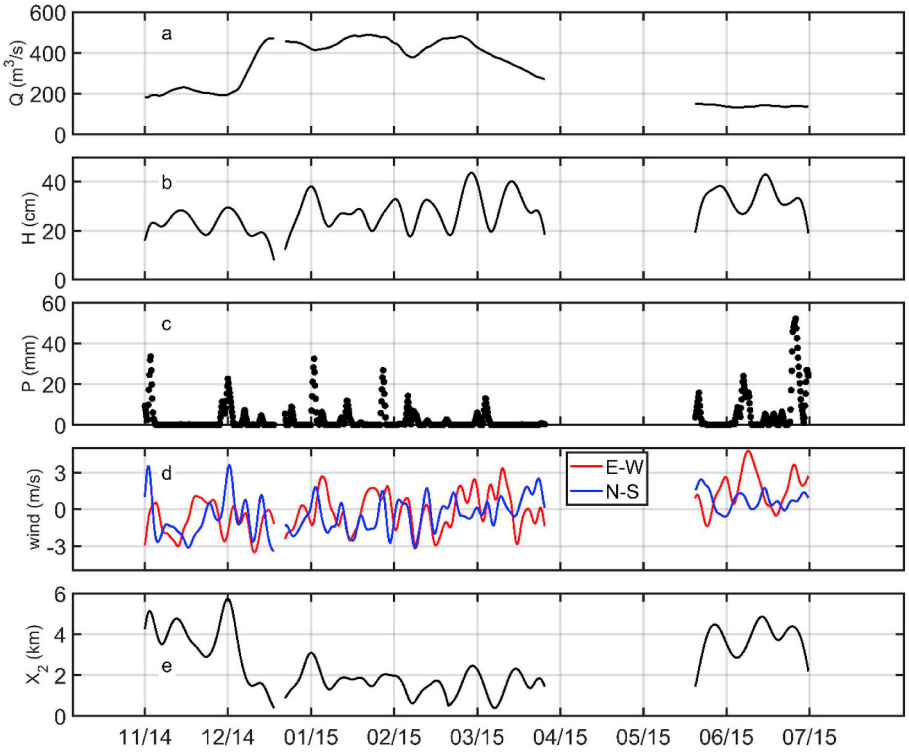

Fig. 3. Training of the Markov-Chain autoregression model, from Nov 23, 2014 to July 21, 2015. a) Smoothed river discharge (m^3/s) with a low-pass Lanczos filter centered at 30hrs; b) Water level (cm) from a semidiurnal complex demodulation; c) Precipitation (mm); d) Wind velocity components in north (blue) and east (red) following the oceanographic convention, smoothed with a low-pass Lanczos filter centered at 70hrs; e) Position of the isohaline of 2 g/kg (X_2) from the linear interpolation. (For interpretation of the references to color in this figure legend, the reader is referred to the Web version of this article.)

$$S(x) = \frac{S_0}{2}\left[1 + tanh\left(\alpha - \frac{x}{\beta(t)}\right)\right], \tag{1}$$

where S_0 is the maximum salinity at the ocean (30 g/kg off the Suwannee River), x is the longitudinal distance in kilometers, α is a nondimensional parameter that establishes the position where sigmoid decay begins in the S distribution, in this case $\alpha = 5$, and $\beta(t)$ is the rate of sigmoid decay in the salinity distribution for each tidal cycle (Warner et al., 2005). At the river boundary, the salinity was taken as $S = 0\ g/kg$ (Chatwin, 1976) and the ocean boundary coincides when $x = 0\ km$. For the hyperbolic tangent interpolation, the length of saltwater intrusion (X_2) was determined by solving $x\ (km)$ in Equation (1) for a salinity of 2 g/kg ($S = 2\ g/kg$).

A first-order Markov chain regression model was applied to time series of X_2, river discharge, water level, precipitation and wind velocity components to determine the saltwater intrusion along the Suwannee River. Estimates of saltwater intrusion were obtained for the period of Nov 23, 2014 to July 21, 2015. Time series of river discharge— $Q(t)$, water level— $H(t)$, precipitation— $P(t)$, and wind velocity components were averaged for each tidal cycle. Time series of the independent variables ($Q(t)$, $H(t)$, $P(t)$, $W_{(east,north)}(t)$) were linearly interpolated to the same time range of the dependent variable— X_2. Discontinuities in the time series (Fig. 2; Fig. 3) occurred between redeployments of the conductivity recorders (CTDs).

Using the methodology of Reyes-Merlo et al. (2013), a first-order Markov chain model was developed to relate any given X_2 to its position in a previous tidal cycle and to the forcings mentioned above. Reyes-Merlo et al. (2013) related X_2 to its location in a previous tidal cycle and to river discharge, tidal current range and easterly wind velocity averaged in the latest tidal cycle. In the case of the Suwannee River, instead of using tidal currents (which were unavailable), the model considers the water level at the mouth, both wind velocity components, and precipitation. Because salinity intrusion is controlled to some extent by river discharge (Tillis, 1999), and the Suwannee River presents a marked seasonality, the analysis was subdivided in high and low river discharge regimes (Simpson et al., 2001). The autoregressive model is defined by:

$$X_2(t) = aX_2(t-1) + bH(t) + cQ(t) + dP(t) + eW_{east}(t) + fW_{north}(t) + g, \tag{2}$$

where the coefficients ($\boldsymbol{b}$, $\boldsymbol{c}$, $\boldsymbol{d}$, $\boldsymbol{e}$, $\boldsymbol{f}$, $\boldsymbol{g}$) are calculated with a least square nonlinear regression for high and low discharge regimes, $X_2(t-1)$ is the isohaline location in a previous tidal cycle (hysteretic term). The coefficient $\boldsymbol{a}$ is attributed to the response time of saltwater intrusion to different forcings. Previous work on the Suwannee river suggests that the river discharge influences saltwater intrusion more than other forcings (Tillis, 1999). The time response was obtained with a lagged cross correlation between river discharge and isohaline position, following:

$$r_x(L) = \frac{\sum_{k=0}^{N-L-1}(Q_k - \bar{Q})(X_{2k+L} - \bar{X}_2)}{\sigma_Q \sigma_{X_2}} = r_x(-L) \tag{3}$$

The numerator has the variations of each variable around their mean ($\bar{Q}$, $\bar{X}_2$), with one of them lagged ($k + L$), and the denominator is the standard deviation of each variable. The lag corresponding to the highest correlation coefficient ($r_x(L)$) indicates the response of saltwater intrusion to changes in river discharge. The time response was obtained with the lag value and the corresponding Δt. This response represents the coefficient $\boldsymbol{a}$ in the autoregressive Markov-chain model. Mathematically, it is given by:

$$a = 1 - \frac{\Delta t}{lag * \Delta t} \tag{4}$$

The coefficient $\boldsymbol{a}$ will be constant, but different for high and low discharge regimes. Discharge regimes were separated by a 250 m^3/s river discharge. This value was selected after a series of trials for river discharges ranging from 200 to 400 m^3/s.

Saltwater intrusion X_2 was projected or predicted for August 8, 2015 to November 23, 2015 using the derived coefficients from the Markov-chain model during the 'training' period of November 2014 to July 2015. The best approach was drawn from either linear interpolation or hyperbolic tangent interpolation, with their corresponding values of the coefficients— $\boldsymbol{b}$, $\boldsymbol{c}$, $\boldsymbol{d}$, $\boldsymbol{e}$, $\boldsymbol{f}$, $\boldsymbol{g}$, for each discharge regime. The CTD deployments corresponding to August–September and

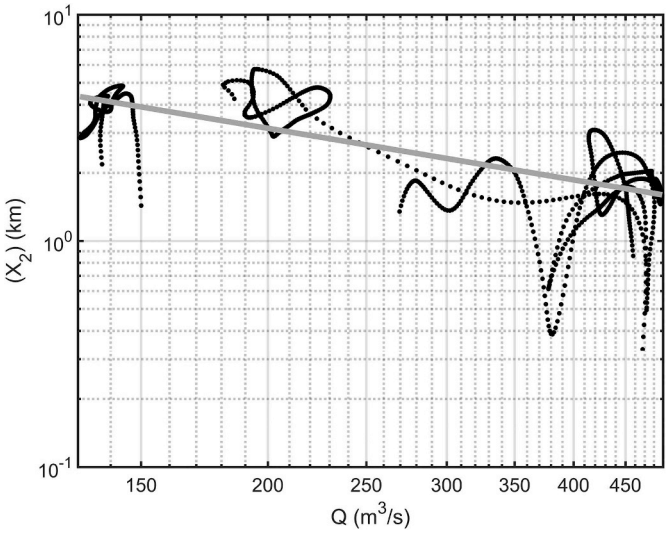

Fig. 4. Power-law relationship between river discharge and X_2 position with the best fit in gray. Location of X_2 from the linear interpolation during the training period (Nov 23, 2014 to July 21, 2015).

October–November 2015 were used to verify the model projections. Interpolated and projected values were compared with the root-mean-square error and goodness of fit, reported in the Results section.

4. Results

This section presents typical salinity distributions along the estuary, and the possible forcings of their variability, namely river discharge, water level, precipitation, and wind. The salinity distribution was obtained from a linear interpolation and a hyperbolic tangent interpolation. A power-law analysis defined the length scale of saltwater due to changes in river discharge. These results are compared with other salt-wedge estuaries. This section includes results from the Markov-chain model and their comparison to observations of saltwater intrusion from both approaches, linear and *tanh* interpolations. The section closes with projections of saltwater intrusion using the model results with the best fit.

4.1. Hydrography

For November 2014 to November 2015, the high river discharge regime coincided with the cold season (Nov–Apr) and had a mean flow of 360 m^3/s. The low river discharge regime overlapped with the warm season (May–Oct) and had a mean flow of 198 m^3/s. The annual mean discharge for November 2014–November 2015 was 340 m^3/s. Annual mean, as well as warm and cold season means considered the uninterrupted data obtained from the USGS station at Wilcox. Compared to mean flows (annual, cold and warm season) from the record 1942–2003, the observed values fall within one standard deviation from their corresponding means. The annual mean flow for the record 1942–2003 was 287 ± 189 m^3/s, the mean flow for the cold season was 320 ± 222 m^3/s, and the mean for the warm season was 255 ± 140 m^3/s (SRWMD, 2005).

The salinity distribution along the Suwannee River was described with a linear interpolation and a *tanh* interpolation. During the time of analysis, the X_2 obtained from the linear interpolation had a similar trend to the water level at the river mouth (Fig. 3b), with greater saltwater intrusion during spring tides than neap tides. Values of X_2 obtained with the linear interpolation fell between stations that recorded salinity values above and below 2 g/kg. The water level amplitude for the semidiurnal band was 30–45 cm for spring tides and decreased to nearly 20 cm at neap tides. The linearly interpolated position of X_2 remained within the first ~6 km from the river mouth from Nov 2014 to July 2015 (Fig. 2; Fig. 3). The position of X_2 described with the *tanh* interpolation reproduced the fortnightly variability of X_2 and the farthest upstream saltwater intrusion coinciding with the low river discharge regime. However, the *tanh* interpolation provided X_2 values that fell upstream from the upper limit of our measurements that indicated salinity of 0 g/kg (Fig. 2). In other words, the *tanh* approach indicated low salinity in locations where the actual salinity was zero (> 10 km from the mouth). The unrealistic estimation of X_2 with the *tanh* interpolation rendered the approach unreliable.

Because the saltwater intrusion at the Suwannee River is better described with the linear interpolation, the following sections refer to that distribution. From the linear interpolation, the greatest X_2 excursion of ~6 km occurred on December 23, 2014 and corresponded to a river discharge of 195 m^3/s. While the shortest excursion reached ~0.40 km when the discharge was 377 m^3/s on March 29, 2015 (Fig. 3). Short saltwater intrusions were restricted to ~2 km from the river's mouth and coincided with river discharges larger than 300 m^3/s.

Precipitation had no evident seasonality, but maximum values of 40–50 mm overlapped with the warm season. There was no clear relationship between changes of precipitation and X_2, but at some instances with no precipitation (November 2014, March 2015, late May 2015), the isohaline position was > 2 km from the mouth. Winds blowing toward the N—W, S—W and SE coincided with X_2 excursions larger than 3 km. The relationship between wind and X_2 was not as clear as that between river discharge and X_2.

The power-law relationship between river discharge and X_2 (from linear interpolation, Fig. 4) indicates, as expected, a decrease of X_2 with an increase of Q. From this power-law relationship, with the river discharge as the independent variable, the Suwannee River estuary empirical relationship, $X_2 \propto Q^n$, has the form of $X_2 = 174\,Q^{-0.76}$ (with coefficients within the 95% confidence interval). The value for n is within the range of high and low regimes (Monismith et al., 2002) but it is closer to $n = -1$, which is associated to high river flows. The salt-wedge estuary of Skagit River estuary in Canada, had a value of $n = -0.25$ reported by Yang and Khangaonkar (2009). For the Modaomen Estuary in China Gong and Shen (2011) reported $n = -0.49$, for constant river discharge. The Modaomen Estuary changes to a salt-wedge estuary during high flow conditions and during spring tides (Gong and Shen, 2011).

4.2. Markov-chain model results

The lagged cross-correlation between river discharge and X_2 shows an inverse relationship (Fig. 5). The maximum lagged correlation coefficient was −0.7 at 1.5 lags, which represents ~7.5 h. From the number of lags and Equation (4), the coefficient $\boldsymbol{a}$ in Equation (2) becomes 1/3. The coefficients— $\boldsymbol{b}, \boldsymbol{c}, \boldsymbol{d}, \boldsymbol{e}, \boldsymbol{f}, \boldsymbol{g}$ of Equation (2) are obtained from a nonlinear least squares regression (nlinfit® Matlab), and are listed in Table 2 for high and low river discharge regimes. The discharge regimes were separated by a Q of 250 m^3/s.

The training of the Markov chain model was successful once the modeled results followed closely the trend of the interpolated X_2 values, capturing all peak values (Fig. 6a). Probability density functions (pdf) for X_2 obtained with the Markov Chain model and the linear interpolation had the same distribution (Fig. 6b). The root-mean-squared error was 0.05 km and the goodness of fit was 87.6%. Modeled results using X_2 from the *tanh* interpolation had a root-mean-squared error of 0.18 km and a goodness of fit of 74%. A scatter plot (Fig. 7) compares both approaches and shows that the Markov-chain model reproduced X_2 better with the linear interpolation. Projections of saltwater intrusion considered the linear interpolation approach because of its agreement with the observed salinity distribution (Fig. 2) and because of its better performance than the *tanh* interpolation.

The model that was trained from November 2014 to July 2015 was used to project the isohaline of 2 g/kg (X_2) from August to November

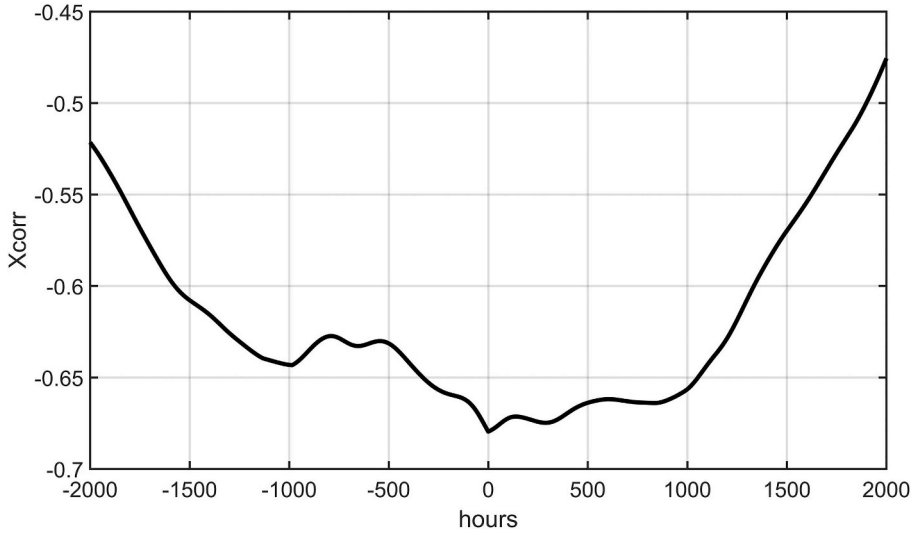

Fig. 5. Lagged cross-correlation between river discharge and the X_2 position from the linear interpolation.

Table 2
Fitting coefficients for high and low river discharge regimes.

	a	b	c	d	e	f	g
low	0.333	0.0644	0.0108	0.0135	−0.0466	0.0791	−1.1290
high	0.333	0.0390	0.0003	0.0147	−0.0416	−0.0013	−0.1368

2015. The projection was then compared to linearly interpolated X_2 locations (from recorded salinity values) over that same period (after August 1, 2015 – vertical dashed line – in Fig. 8). The Markov-chain model used the constant value for coefficient $\boldsymbol{a}$ and the fitted coefficients, all listed in Table 2. Salinity measurements were available from two deployments, August–September and October–November 2015. As shown in Fig. 8, the autoregressive model follows the trend of X_2, for a river discharge below average, X_2 excursion is larger, > 4 km upstream. For the deployment from October to November 2015, the model reproduced almost exactly the X_2 location. The goodness of fit for the projection period (August–November 2015) was 61% and the root-mean-square error was 7 km.

5. Discussion

It is evident that the saltwater intrusion has seasonal variability, changing from low discharge to high discharge seasons; and closely depends on the isohaline position from the previous tidal cycle. This response has also been reported in temperate estuaries, such as the Mississippi River estuary, USA (Mann, 2000), and the Yura estuary, Japan (Kasai et al., 2010). For a subtropical and salt-wedge estuary, the longitudinal salinity distribution was well represented with a linear interpolation. The inverse proportionality between the isohaline position and the river discharge was also observed in a fluvially dominated portion of the Upper Suwannee River from August 1995 to December 1997 (Tillis, 1999). Basically, maxima isohaline upstream excursions coincided with low river flows. In that sense, the saltwater intrusion was not intensified during seasonal high flows but might be intensified during shorter times scales, like strong river pulses described in Valle-Levinson (2012).

From the power-law relationship between the river discharge and the isohaline position (Fig. 4), the exponent ($n = -0.76$) is closer to $n = -1$ than to 0.1. This proximity of n to unity suggests that salt transport is dominated by tidal oscillatory dispersion and not by

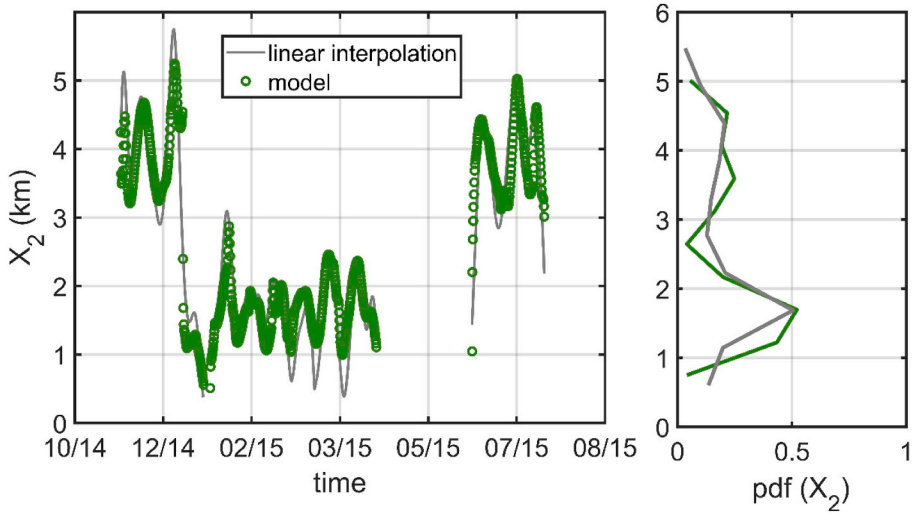

Fig. 6. Model results for the X_2 position from November 2014 to July 2015. a) Linear interpolated X_2 values in gray lines and model X_2 values in green circles; b) Probability density function for the linearly interpolated (gray line) and modeled values (green line). RMS error = 0.05 km; R^2 = 87.6%. (For interpretation of the references to color in this figure legend, the reader is referred to the Web version of this article.)

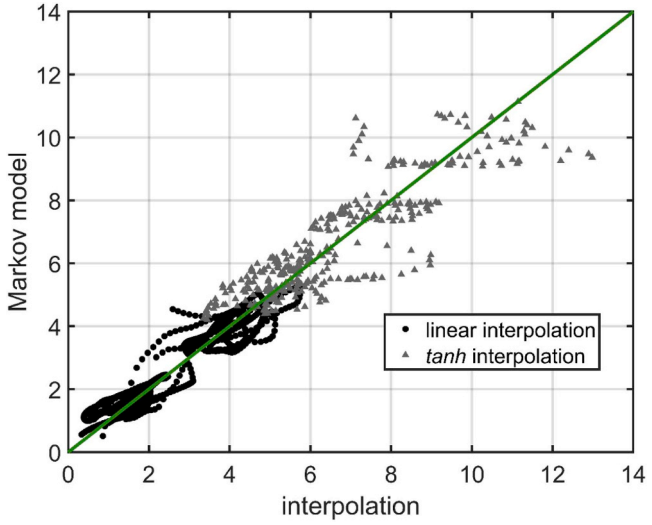

Fig. 7. Markov modeled X_2 vs linear and *tanh* interpolated X_2. 1-1 line in green. (For interpretation of the references to color in this figure legend, the reader is referred to the Web version of this article.)

gravitational circulation (Abood, 1974; Monismith et al., 2002; Bowen and Geyer, 2003). A value of $n = -1$ also indicates that during high river discharge the saltwater intrusion is strongly related to river discharge (Monismith et al., 2002). Other studies in salt-wedge estuaries have reported smaller values for n, i.e. the Skagit River estuary has an $n = -0.25$ but its river flow is regulated by upstream hydropower dams. The Modaomen Estuary in China has shown a value of $n = -0.49$ from numerical simulations, for a constant river discharge.

The Markov chain model does a reasonable job reproducing the length of saltwater intrusion. The excursion of salt water in a salt-wedge estuary is well explained by the variability of the river discharge, subtidal water level, precipitation and wind components. From August to September 2015, the saltwater intrusion was shorter than what the model predicted. A possible explanation of this discrepancy could be the influence of local rainfall events on the saltwater intrusion. These predictions were anchored on one precipitation station. Future efforts should consider the spatial variability of rainfall in the river basin to assess whether the model is sensitive to such variations. Based on the results from the Markov chain model and its coefficients, the most important term in predicting X_2 is the memory term $X_2(t-1)$. From Table 2, the coefficient $a = 0.333$ is larger than the other coefficients, for high and low discharge regimes. The same response was documented in a temperate estuary of southern Spain (Reyes-Merlo et al., 2013). Response time from the Suwannee River was 7.5 h, less than a semidiurnal tidal cycle. This fast response can be attributed to the river's slope and depth. MacCready (1999) reported fast adjustment times for shallow and also for deep estuaries. The Suwannee River is a low-gradient stream with mean depths of ~7 m, but the estuarine portion has mean depths < 3 m.

The autoregressive model can further be used to forecast possible values of saltwater intrusion in the Suwannee River, a subtropical estuary, for different combinations of river discharge variations and sea level rise. Even though saltwater intrusion is aggravated by human pressure (e.g., extraction of groundwater, coastal development), it can be intensified by sea level rise and associated storm surges (Wong et al., 2014). According to the IPCC, increases in sea level are expected to range from 0.25 to 1 m (Church et al., 2013). Coastal and riverine communities that consume water directly from river sources without any treatment are facing health complications due to saltwater intrusion (Khan et al., 2011; Vineis et al., 2011). According to the World Health Organization (WHO) and the Environmental Protection Agency (EPA), there is no guideline for safe salinity levels in drinking water.

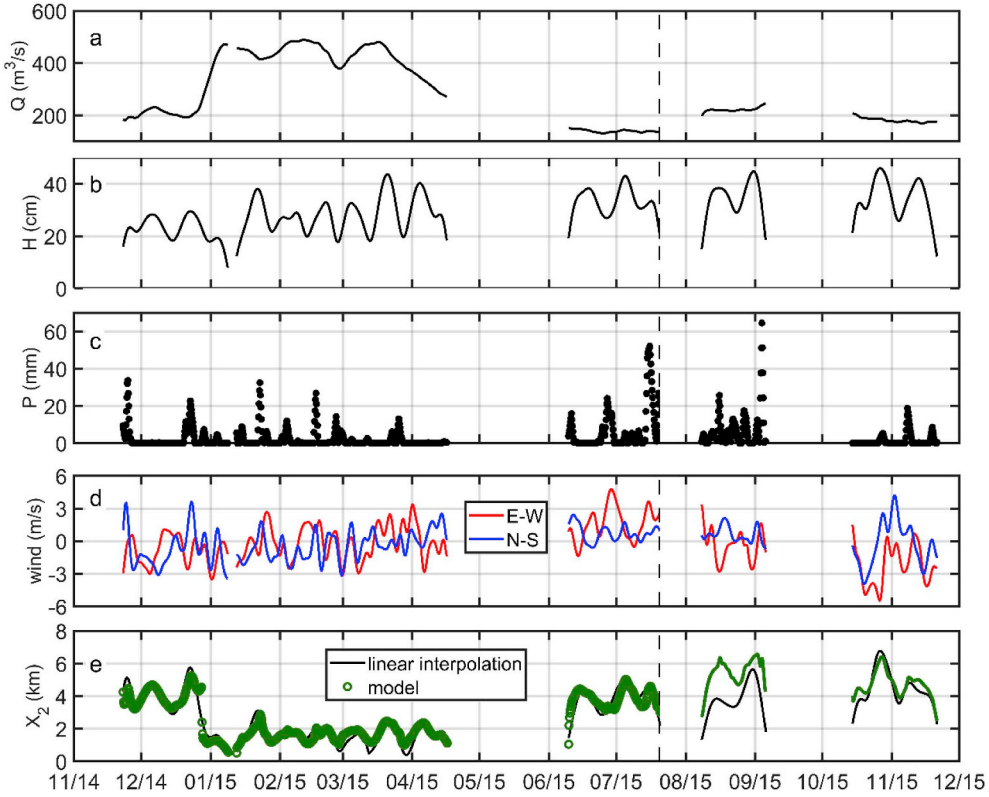

Fig. 8. Projection of the position of X_2 for August 8 to November 23, 2015. a) River discharge (m^3/s); b) Water level (cm); c) Precipitation (mm); d) Wind velocity components (m/s); e) Position of the isohaline of 2 g/kg (X_2), with linear interpolated positions in black and projections in green. (For interpretation of the references to color in this figure legend, the reader is referred to the Web version of this article.)

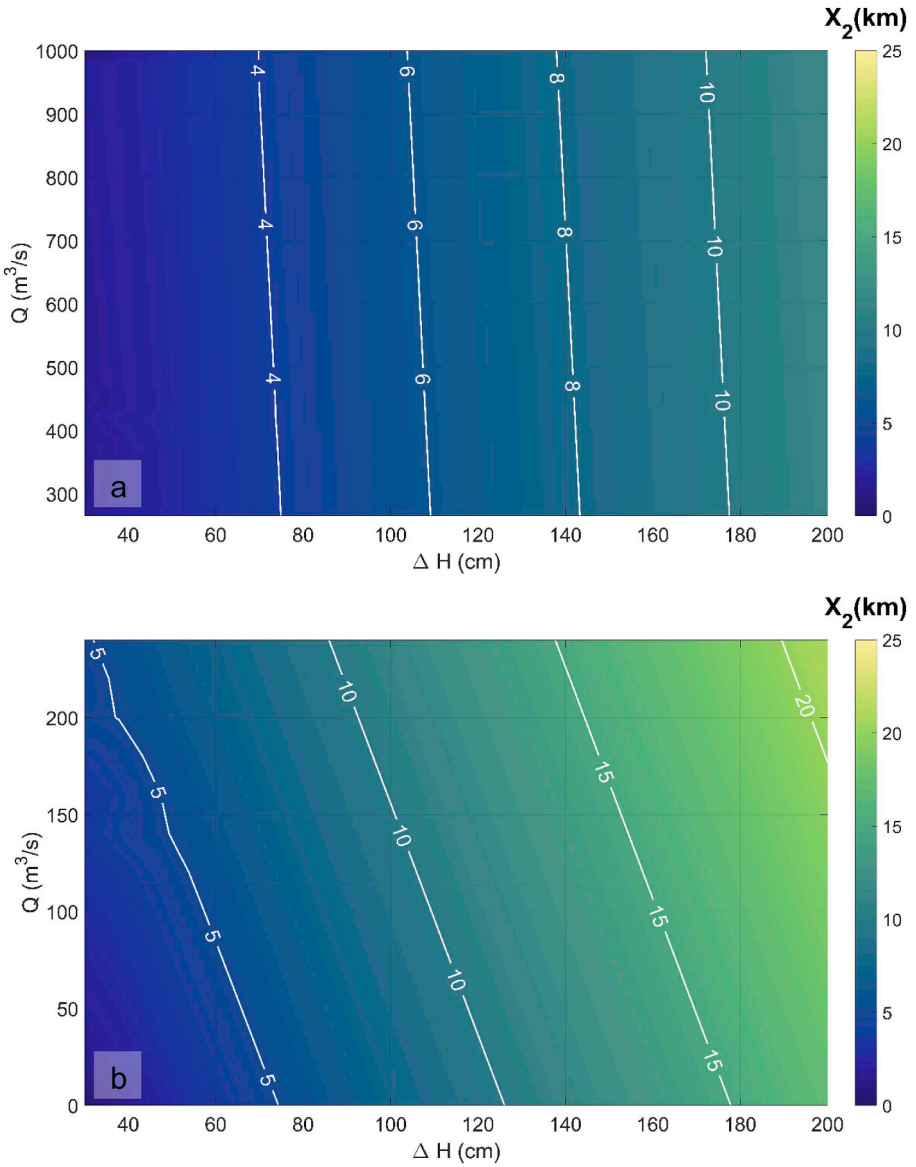

Fig. 9. Projections of saltwater intrusion in terms of X_2 location for changes in river discharge (m^3/s) and water level (cm), a) river discharge of 250–1000 m^3/s and b) river discharge of 0–250 m^3/s.

Both organizations have not established direct levels of salinity. Instead, concentrations of Sodium or Chloride are listed under non-enforceable Secondary Drinking regulations (EPA, 2008). In rural coastal Bangladesh, prevalence of hypertension in pregnant women was attributed to increased levels of sodium from drinking water during the dry season. Levels of sodium intake exceed recommended limits (Khan et al., 2011). Besides the human health implications of saltwater intrusion, the production of freshwater wetlands will decline. For instance, biomass and growth of several freshwater wetlands declined 55% for increased salinities while for larger freshwater inputs the production increased by 75% (Neubauer, 2013).

For the above reasons, it is necessary to make projections about saltwater intrusion, at local and regional scales especially in low-lying coastal areas. The Markov chain model was used to project X_2 for different river discharge values and increases of water level (Fig. 9). Using the coefficients for high and low discharge regimes, the Markov chain model projected the isohaline position for river discharge ranging from 0 to 1000 m^3/s and increases of water level (sea-level rise values) from 30 to 200 cm at the mouth. The position of the X_2 is expressed in kilometers from the mouth. Initial values of X_2, derived from the Markov-chain model results, have corresponding values of river discharge and water level. These initial conditions correspond to the zero increase in water level and are located at the right-most part of each panel in Fig. 9. For river discharge between 0 and 250 m^3/s, and a fixed water level (x-axis), the saltwater intrusion mainly depends on changes of river discharge. For a river discharge between 250 and 1000 m^3/s, the saltwater intrusion will mainly respond to changes of water level at the mouth.

As expected, the greatest excursion of the X_2 isohaline was 20 km for river discharge lower than 250 m^3/s and for a water level higher than 170 cm. For a river discharge greater than 250 m^3/s the maximum value of X_2 was 10 km for an increase in water level > 150 cm. These projections support the statement that saltwater intrusion is dominated by changes in river flow, commonly observed in temperate estuaries. Estuaries from tropical and subtropical regions, like the Suwannee River estuary, are essentially unexplored in comparison to higher latitudes estuaries. This study elucidates saltwater intrusion lengths and their linkage to possible forcings in a subtropical estuary. Information is needed from many other estuaries to narrow conclusions within subtropical and tropical regions. Projections of saltwater intrusion that

consider different scenarios of sea-level rise and river discharge are key findings for low-lying coastal areas around the globe.

6. Conclusions

The location of the isohaline of 2 g/kg (X_2) in a subtropical, salt-wedge, fast-response estuary was best described using linear interpolation and predicted using a first order Markov-chain autoregressive model. The acceptable performance of the model considered river discharge, water level, precipitation and wind velocity components. The approach of subdividing the discharge regimes in high and low indicated the inverse proportionality of saltwater intrusion to river discharge. Longest (~6 km) saltwater intrusions appeared during the low river discharge regime. Saltwater intrusion in the Suwannee River is expected to increase 2–3 times under the expected scenarios of sea-level rise and river discharge. This estimation of saltwater intrusion will be valid if the independent variables (river discharge, wind, water level, and precipitation) maintain a constant distribution. If these distributions change, this type of model will need to be re-trained. Water managers, stakeholders, ecologists and public health organizations could adapt this type of models in other systems to forecast saltwater intrusion scenarios and the medium-term sustainability of water resources.

Acknowledgements

The study was supported by the Institute of International Education through their Global Innovation Initiative. GEGC thanks the support from Secretaría Nacional de Ciencia y Tecnología (SENACYT) from Panamá for her PhD studies. AVL acknowledges support from the NSF Project 1332718.

References

Abood, K.A., 1974. Circulation in the Hudson estuary. Ann. N. Y. Acad. Sci. 250, 39–111.
Bowen, M.M., Geyer, W.R., 2003. Salt transport and the time-dependent salt balance of a partially stratified estuary. J. Geophys. Res. 108.
Chatwin, P.C., 1976. Some remarks on the maintenance of the salinity distribution in estuaries. Estuar. Coast Mar. Sci. 555–566.
Church, J.A., Clark, P.U., Cazenave, A., Gregory, J.M., Jevrejeva, S., Levermann, A., et al., 2013. 2013: sea Level change. In: Climate Change 2013: the Physical Science Basis. Contribution of Working Group I to the Fifth Assessment Report of the Intergovernmental Panel on Climate Change. Cambridge University Press, Cambridge, United Kingdom and New York, NY, USA.
Crain, C.M., Silliman, B.R., Bertness, S.L., Bertness, M.D., 2004. Physical and Biotic drivers of plant distribution across estuarine salinity gradients. Ecology 85 (9), 2539–2549.
Crandall, C.A., Katz, B.G., Hirten, J.J., 1999. Hydrochemical evidence for mixing of river water and groundwater during high-flow conditions, lower Suwannee River basin, Florida, USA. Hydrogeol. J. 7, 454–467.
EPA, 2008. Guidelines for Drinking-water Quality. Incorporating the First and Second Addenda, vol. 1 World Health Organization, Geneva.
Fischer, H.B., 1976. Mixing and dispersion in estuaries. Annu. Rev. Fluid Mech. 8, 107–133.
Gong, W., Shen, J., 2011. The response of salt intrusion to changes in river discharge and tidal mixing during the dry season in the Modaomen Estuary, China. Continent. Shelf Res. (31), 769–788.
Hansen, D.V., Rattray, M., 1965. Gravitational circulation in straits and estuaries. J. Mar. Res. 23, 104–122.
Hetland, R.D., Geyer, W.R., 2004. An idealized study of the structure of long, partially mixed estuaries. J. Phys. Oceanogr. 34, 2677–2691.
Jassby, A.D., Kimmerer, W.J., Monismith, S.G., Armor, C., Cloern, J., Powell, T., et al., 1995. Isohaline position as a habitat indicator for estuarine populations. Ecol. Appl. 5 (1), 272–289.
Kasai, A., Kurikawa, Y., Ueno, M., Robert, D., Yamashita, Y., 2010. Salt-wedge intrusion of seawater and its implication for phytoplankton dynamics in the Yura Estuary, Japan. *Estuarine*. Coastal and Shelf Science (86), 408–414.
Katz, B.G., DeHan, R.S., Hirten, J.J., Catches, J.S., 1997. Interactions between ground water and surface water in the Suwannee River Basin Florida. J. Am. Water Resour. Assoc. 33 (36), 1237–1254.
Khan, A.E., Ireson, A., Kovats, S., Mojumder, S.K., Khusru, A., Rahman, A., et al., 2011. Drinking water salinity and maternal health in coastal Bngladesh: implications of climate change. Environ. Health Perspect. 119 (9), 1328–1332.
Kranenburg, C., 1986. A time scale for long-term salt intrusion in well-mixed estuaries. J. Phys. Oceanogr. 16 (7). https://doi.org/10.1175/1520-0485(1986)016<1329:ATSFLT>2.0.CO;2.
Lerczak, J.A., Geyer, W.R., Chant, R.J., 2006. Mechanisms driving the time-dependent salt flux in a partially stratified estuary. J. Phys. Oceanogr. 36 (12), 2296–2311. https://doi.org/10.1175/JPO2959.1.
Lerczak, J.A., Geyer, W.R., Ralston, D.K., 2009. The temporal response of the length of a partially stratified estuary to changes in river flow and tidal amplitude. J. Phys. Oceanogr. 39 (4), 915–933. https://doi.org/10.1175/2008JPO3933.1.
Light, H.M., Darst, M.R., Lewis, L.J., Howell, D.A., 2002. Hydrology, Vegetation, and Soils of Riverine and Tidal Floodplain Forests of the Lower Suwannee River, Florida, and Potential Impacts of Flow Reductions. U.S. Geological Survey Professional Paper 1656-A, pp. 124.
MacCready, P., 1999. Estuarine adjustment to changes in river flow and tidal mixing. J. Phys. Oceanogr. 29, 708–726.
MacCready, P., 2007. Estuarine adjustment. J. Phys. Oceanogr. 2133–2145.
Mann, K.H., 2000. Ecology of Coastal Waters. Blackwell Science, Massachusetts.
McDougall, T.C., Jackett, D.R., Millero, F.J., Pawlowicz, R., Barker, P.M., 2012. A global algorith for estimating Absolute Salinity. Ocean Sci. (8), 1123–1134.
McDougall, T.J., Barker, P.M., 2011. Getting started with TEOS-10 and the gibbs seawater (GSW) oceanographic toolbox. SCOR/IAPSO WG127, 28.
McPherson, B., Hammett, K., 1991. Tidal Rivers of Florida.
Monismith, S.G., Kimmerer, W., Burau, J.R., Stacey, M.T., 2002. Structure and flow-induced variability of the subtidal salinity field in northern san francisco Bay. J. Phys. Oceanogr. (32), 3003–3019.
Neubauer, S., 2013. Ecosystem response of a tidal freshwater marsh experiencing saltwater intrusion and altered hydrology. Estuar. Coast 36, 491–507.
Pritchard, D.W., 1954. A Study of Flushing in the Delaware Model. Chesapeake Bay Institute.
Reyes-Merlo, M.Á., Díez-Minguito, M., Ortega-Sánchez, M., Baquerizo, A., Losada, M.Á., 2013. On the relative influence of climate forcings agents on the saline intrusion in a well-mixed estuary: medium-term Monte Carlo predictions. In: Proceedings 12th International Coastal Symposium Plymouth, England, pp. 1200–1205 (Journal of Coastal Research).
Simpson, J.H., Vennell, R., Souza, A.J., 2001. The salt fluxes in a tidally-energetic estuary. *Estuarine*. Coastal and Shelf Science (52), 131–142.
SRWMD, 2005. Establishment for the Lower Suwannee River & Estuary, Little Fanning, Fanning, and Manatee Springs.
Thomson, R.E., Emery, W., 2014. Data Analysis Methods in Physical Oceanography, third ed. .
Tillis, G.M., 1999. Flow and Salinity Characteristics of the Upper Suwannee River Estuary. USGS, Florida.
Tootle, G.A., Piechota, T.C., 2004. Suwannee river long range streamflow forecasts based on seasonal climate predictors. J. Am. Water Resour. Assoc. 40 (42), 523–532.
Tuckey, T.D., Dehaven, M., 2006. Fish assemblages found in tidal-creek and seagrass habitats in the Suwannee River estuary. Fish. Bull. 104, 102–117.
Valle-Levinson, A., 2012. Impact of record flooding of a subtropical river on estuary/ocean exchange. Ocean Dynam. 62, 77–85.
Vineis, P., Chan, Q., Khan, A., 2011. Climate change impacts on water salinity and health. J. Epidemiol. Global Health (1), 5–10.
Warner, J.C., Geyer, W.R., Lerczak, J.A., 2005. Numerical modeling of an estuary: a comprehensive skill assessment. J. Geophys. Res. https://doi.org/10.1029/2004JC002691.
Wong, K.-C., Valle-Levinson, A., 2002. On the relative importance of the remote and local wind effects on the subtidal exchange at the entrance to the Chesapeake Bay. J. Mar. Res. 22, 477–498.
Wong, P.P., Losaza, I.J., Gattuso, J.-P., Hinkel, J., Khattabi, A., McInnes, K.L., et al., 2014. Coastal systems and low-lying areas. In: Climate Change 2014: IMpacts, Adaptation, and Vulnerability. Cambridge Press, Cambridge.
Yang, Z.Q., Khangaonkar, T., 2009. Modeling tidal circulation and stratification in Skagit River estuary using an unstructured grid ocean model. Ocean Model. (28), 34–49.